Electronic Supplementary Material (ESI) for Chemical Science.

Supplementary Information

Modulation of IL-17 backbone dynamics reduces receptor affinity and reveals a new inhibitory mechanism.

Daniel J. Shaw[a], Lorna C. Waters[b], Sarah L. Strong[b], Monika-Sarah E. D. Schulze[c], Gregory M. Greetham[d], Mike Towrie[d], Anthony W. Parker[d], Christine E. Prosser[c], Alistair J. Henry[c], Alastair D. G. Lawson[c], Mark. D. Carr[b], Richard J. Taylor[c], Neil T. Hunt*[a] and Frederick W. Muskett*[b]

a. Department of Chemistry and York Biomedical Research Institute, University of York, Heslington, York, YO19 5DD, UK
b. Department of Molecular and Cell Biology/Leicester Institute of Structural and Chemical Biology, University of Leicester, University Road, Leicester, LE1 7RH, UK.
c. UCB Pharma, UCB Biopharma UK, 216 Bath Road, Slough, SL1 3WE, UK
d. Central Laser Facility, Research Complex at Harwell, STFC Rutherford Appleton Laboratory, Harwell Oxford, Didcot, Oxon, OX11 0QX, UK

Methods:

2D-IR spectroscopy. For 2D-IR measurements, 20 μL of IL-17 solution was held between two CaF_2 windows, separated by a 25 μm thickness spacer. The IL-17 solutions (~ 100 μM) also contained 50 mM Sodium Phosphate, 100 mM NaCl, pH 7.4 buffer. It is noted that, at the concentrations used, <200 μM for MC, any IR absorption bands of the free MC in the region studied are not observed.

All 2D-IR and infrared pump-probe spectra were acquired using the ULTRA B laser system at the STFC Rutherford Appleton Laboratory, which has been described elsewhere[1]. The Fourier Transform 2D-IR method in which three mid infrared wavelength pulses are arranged in a quasi-pump-probe configuration comprising a pair of collinear pump pulses and a probe pulse was used. The mid IR laser pulses had a <100 fs pulse duration and a bandwidth of >300 cm^{-1}, centred at 1650 cm^{-1}. The time delay between the two pump pulses, τ, was controlled by an interferometer. The waiting time (T_w) was controlled by a second optical delay line. A mechanical chopper set to half the repetition rate of the laser (10 kHz) was used to remove residual pump-probe signals. To account for laser power fluctuations, the signal was normalized using a static reference beam. Each 2D-IR spectrum is the average of three scans, with a spectral resolution of 1.8 cm^{-1} along the pump frequency axis. The probe frequency axis of the 2D-IR spectrum was measured with a spectral resolution of 1.4 cm^{-1} using a spectrograph and HgCdTe array detector. The polarisation relationship between pump and probe beams was parallel.

NMR Spectroscopy. NMR spectra of the IL-17 dimers were acquired from 350 μl samples of approximately 200 μM monomer IL-17AA, and IL-17FF, and 75-100 μM protomer IL-17AF (only one protomer labelled) in a 20 mM sodium phosphate, 100 mM sodium chloride and 3mM sodium azide buffer at pH 6.0, containing 5% D_2O/95% H_2O. NMR spectra of the IL-17 hetero-dimers with macrocycle (at 1.5 molar equivalents) were acquired from 350 μl samples of 200 μM $^{15}N/^{13}C/^{2}H$ labelled IL-17A in complex with unlabelled IL-17F and 110-200 μM unlabelled IL-17A in complex with $^{15}N/^{13}C/^{2}H$ labelled IL-17F in a 20 mM sodium phosphate, 100 mM sodium chloride and 3mM sodium azide buffer at pH 6.0, containing 5% D_2O/5% d_6-DMSO/90% H_2O.

NMR data were acquired at 308K on either a 600 MHz Bruker Avance HD III or 800 MHz Bruker AVII spectrometer equipped with 5mm, z-gradient TCI cryoprobes. Spectra assignments for the apo-IL-17 homo- and hetero- dimers have been reported previously[3]. The 2D and 3D spectra recorded to obtain sequence specific assignments for IL-17AF hetero-dimer with MC were in-house versions of: $^{15}N/^{1}H$ TROSY; NOESY-TROSY with an NOE mixing time of 200 msec, and TROSY versions of $^{15}N/^{13}C/^{1}H$ HNCACB, HN(CO)CACB, HNCA and HNCO (reviewed in[4]) with labelled IL-17A/unlabelled IL-17F and *vice versa*. The $^{15}N/^{1}H$ NOESY-TROSY and $^{15}N/^{13}C/^{1}H$ triple resonance experiments (except the TROSY-HNCO for labelled IL-17A/unlabelled IL-17F) were acquired using non-uniform sampling, with the datasets sparsed at 40-44% and 27% respectively. The majority of the 3D spectra were collected over approximately 64-90 hours. The WATERGATE method was used to suppress the water signal when required[5]. In addition, 2D double filtered NOESY experiments[6] were acquired to record NOEs between unlabelled protomers and the macrocycle.

^{15}N relaxation data were acquired on a Bruker AV III HD 600MHz spectrometer using in-house written, standard TROSY based T_1, T_2 and NOE experiments[7-8]. Typical acquisition times were 60 msec for ^{15}N (F_1) and 80 msec ^{1}H (F_2), with relaxation delays as follows: T_1 48, 120, 224, 360, 528,728 and 960 msec; T_2 4.8, 9.6, 28.2, 48, 72, 101 and 134 msec. Two time points in each series were repeated in order to estimate errors. The overall delay in NOE experiments was 4.5sec, and the CPMG pulse train delay was set to 0.45 msec.

All NMR data were processed using NMRPipe[9] with linear prediction used to extend the effective acquisition times by up to 2-fold in nitrogen in regular sampled data. The non-uniform sampled data was reconstructed using the IST algorithm implemented in NMRPipe. The HSQC spectra were referenced to water at 308K. Spectra were analysed, and relaxation parameters calculated, using the NMRFAM Sparky package[10]. R_1 and R_2 values were calculated by fitting a single exponential decay function to the peak height measurements (intensity) against relaxation delay. Uncertainty in peak height was determined from duplicate spectra, and errors in R_1 and R_2 estimated by generating Gaussian random distributions of the peak intensities and repeating the fits many times. The $\{^{1}H\}$-^{15}N heteronuclear NOE values were calculated as:

$$NOE = Isat/Ieq$$

Where Isat and Ieq are the intensities of a peak in the spectra collected with and without proton saturation. Uncertainties in the hetNOE values were estimated using established methods[11].

Values for the reduced spectral density function were calculated using the software Relax version 4.1.3[12-13]. The program Prism was used for graphical analysis of the results, and Pymol for representation of the crystal structures. Median values were calculated for all relaxation parameters and reduced spectral density functions and any value more than one median average difference were considered to be significantly different.

Biolayer Interferometry Binding Assays. The dissociation constant (K_D), K_{on} and K_{off} for IL-17AA and IL-17AF binding to IL-17RA were determined by biolayer interferometry on an Octet QKe system (ForteBio). Equivalent experiments were also recorded in the presence of a saturating amount of MC. Protein samples were diluted in PBS (137 mM NaCl, 10 mM Na_2HPO_4, 1.8 mM KH_2PO_4) pH 7, 0.05% (v/v) Tween 20 and 0.1% BSA. Diluted IL-17AA and IL-17AF samples were incubated in the presence of either 3.5% (v/v) DMSO or 3.5% (v/v) DMSO and 175 µM MC at room temperature for 48 hours prior to the BLI experiments. Experiments were carried out at 25°C and 1000rpm orbital shaking.

Protein G biosensors were preequilibrated in PBS pH 7, 0.05% (v/v) Tween 20 and 0.1% BSA in order to obtain a baseline. The biosensors were then coated with C-terminal Fc tagged IL-17RA (residues 33-320) (R&D Systems) at 5 µg/ml for 350s, or a negative control of just buffer. A second baseline was then recorded for 60s in PBS pH 7, 0.05% (v/v) Tween 20, 0.1% BSA and 3.5% (v/v) $DMSO_4$. During the association step IL-17RA was titrated with increasing concentrations of untagged IL-17AA or His-IL-17AF (0, 2.5, 5, 10, 20, 40, 80, 160 nM) for 1500 s. For the dissociation stage the biosensors were then returned to the wells used for the second baseline step for 1500 s. For experiments looking at the effect of the MC on the interaction of either IL-17AA or IL-17AF with IL-17RA, 175µM MC was present in the wells used for the second baseline, association and dissociation steps.

Raw data was corrected by double referencing and analysed using the Octet data analysis software (ForteBio) were exported into Prism (version 9.3.1). The K_D values were derived from the steady state equilibrium analysis by fitting the steady state maximum response binding levels observed for the range of IL-17 concentrations analysed. Association and dissociation rate constants were calculated based on fitting to the heterogeneous ligand model in the Octet Data Analysis software (version 12.0.2.11).

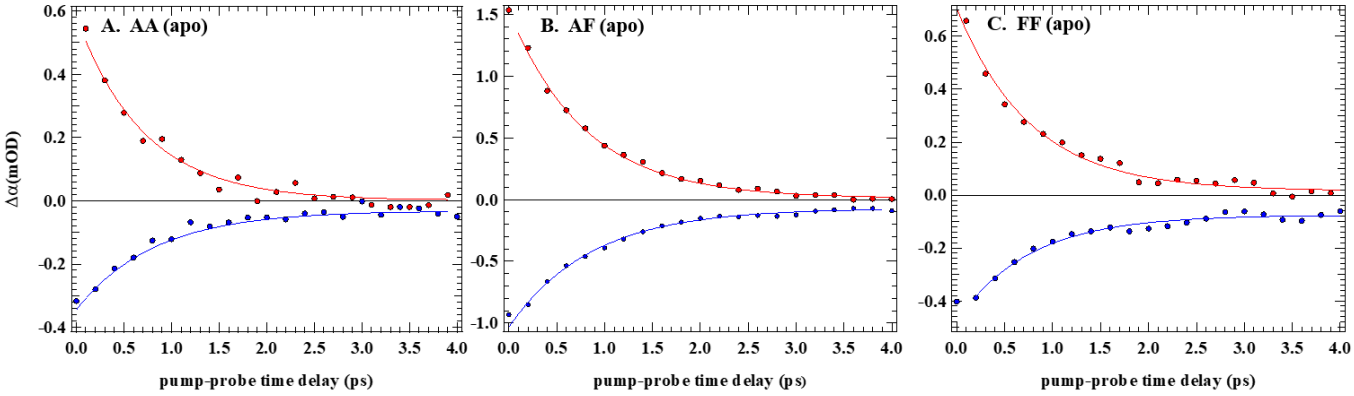

Figure S1: Infrared pump-probe data showing vibrational dynamics for the ground state recovery (blue) and excited state relaxation (red) for the amide I band of **A.** apo- IL-17AA, **B.** IL-17AF and **C.** IL-17FF recorded using a parallel pump-probe geometry in which the rotational contribution to the relaxation is effectively zero given the large size of the protein molecule (~33 kDa) and the very short timescale of the vibrational relaxation (<1ps) of the protein. The data in all three cases is well described by fitting to a mono-exponential rise or decay function. This yields lifetimes of 0.87 ± 0.08 ps and 0.65 ± 0.07 fs for the IL-17AA ground and excited state**s;** 0.81 ± 0.04 ps and 0.79 ± 0.03 ps in the case of IL-17 AF, and 0.74 ± 50 ps and 0.77 ± 0.03 ps for IL-17FF respectively.

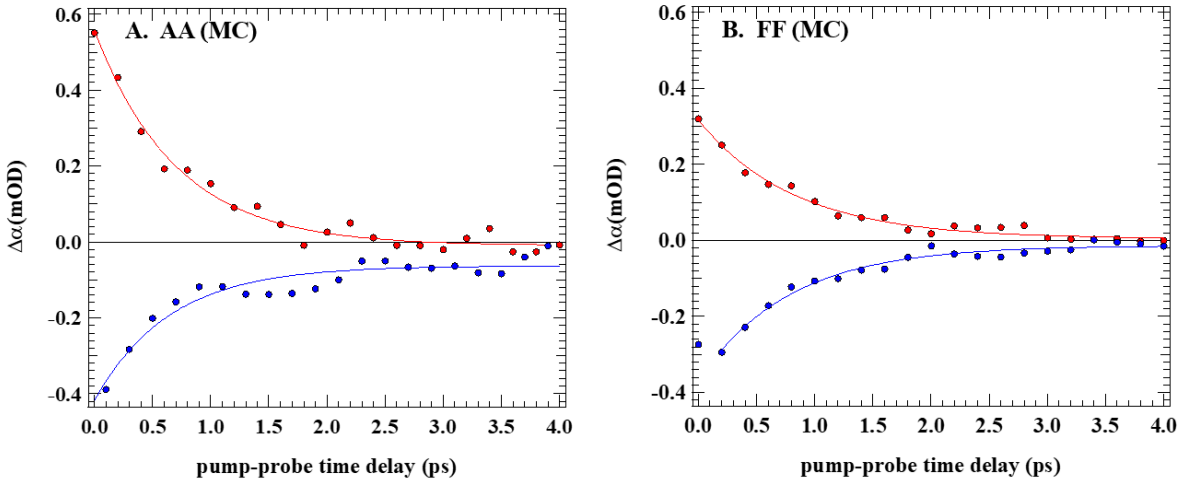

Figure S2: Infrared pump-probe data showing vibrational dynamics for the ground state recovery (blue) and excited state relaxation (red) for the amide I band of **A.** macrocycle-bound IL-17AA and **B.** IL-17FF under the same polarization geometry (parallel probe and pump) as stated in Figure S1. In the case of IL-17AA, the two-fold addition of the macrocyclic compound results in a decrease in the ground and excited state lifetimes obtained for the apo-form to 0.70 ± 0.04 ps and 0.65 ± 0.07 ps respectively. Conversely, the same MC addition to IL-17FF results in no observable change in lifetime when compared to IL-17FF(apo-), yielding ground and excited state relaxation times of 0.78 ± 0.05 ps and 0.83 ± 0.05 ps respectively.

NMR Spectroscopy.

For IL-17AA, of the 90 backbone amide resonances assigned (75.6%) in the ^{15}N-TROSY spectrum, 57 could be used to calculate relaxation parameters. Values of R_1 and R_2 are moderately uniform between residues 65 and 155, however the N- terminal region has significantly elevated R_1 and decrease R_2 values (indicating psec-nsec flexibility and/or anisotropic rotation) compared to the majority of residues of the core β-hairpins. These regions also have reduced heteronuclear NOE, again indicating internal flexibility (τ_e). The C- terminal residues 139 to 148 have more core like values with the last few residues being significantly smaller. The reduced values of R_2 and heteronuclear NOE suggest considerable backbone flexibility in these regions. Both the N- and C- termini are effectively tethered to the core of the protein *via* the disulphide bonds in the cysteine knot (residues C94-C144 and C99-C146) and the interchain disulphide between residues C33 and C129. These disulphide bonds stabilize the backbone motions in the adjacent residues, but the affect is limited particularly in the N-terminal which shows internal flexibility up to about residue 40.

Analysis of the relaxation data using reduced spectral density mapping (see Figure S5) shows that J(0) values are not particularly uniform within the IL-17AA homodimer, with the N- and C- termini showing significant deviations, and the core β-hairpins showing some non-uniformity. Significantly elevated values of J(0) can indicate conformational exchange however, exchange contributions can be obscured by increased flexibility on the psec-nsec timescale and by motional anisotropy. The observation that the IL-17AA isoform has a hydrophobic core that is considerably more dynamic is supported by the 2D-IR data, were the β-sheet signal is not clearly separated from the main amide I band leading to a single 'averaged' frequency distribution (see Figure 1, main text).

Reduced values of J(0) and elevated values of $J(0.87\omega_H)$ at the N- and C- termini indicate fast internal motion (τ_e) on the psec-nsec timescale which is observed in many proteins. Identification of residues exhibiting such motions is achieved with the $J(0.87\omega_H)$ *vs* J(0) plot (See Figure S6) where, in this study, residues whose $J(0.87\omega_H)$ values is more than one median average deviation from the median value are considered to exhibit fast internal motion. These residues also exhibit a left shift in the $J(\omega_N)$ *vs* J(0) plot (see Figure S7), again indicative of fast internal motions (whereas a right shift would indicate chemical exchange in the μsec-msec timescale). In the absence of a well-defined model of motion, τ_e is not readily interpretable as it is related to both rate and amplitude of internal motions that are faster than τ_c. However, for this study fast internal motions are those associated with regions of little or no regular secondary structure that make limited, or only transient, interactions with the core protein.

For the residues that reliable relaxation parameters could be measured, none showed significantly elevated values of J(0) (*i.e.,* greater than the median average deviation) indicating that none of these residues are in conformational exchange. This is reflected in $J(\omega_N)$ *vs* J(0) plot (Figure S7) in which no residues exhibit a right shift. Although relaxation parameters could not be calculated for the 26 residues who's signals decay very rapidly during the experiments, it is not unreasonable to assume this is due to significant conformational exchange. Using the above analysis, residues can be categorized as their relaxation being dominated by the proteins overall correlation time (τ_c), fast internal motions (τ_e) or conformational exchange (R_{ex}).

Viewed on the structure of IL-17AA the backbone dynamics of the molecule start to become clearer (see Figure 2 main text, and Figure S8). The 'collar' region and the top of the 'body' and 'sleeves' are the most stable parts of the protein. However, the lower part of the 'body' and the 'skirt' region appear to be in conformational exchange. Strand 2 of the first β-hairpin also has a region of residues that appear to be in conformational exchange, however this could be due to the proximity of this region to the second β-hairpin that is in conformational change rather than a reflection of actual conformational exchange of these residues.

For the IL-17FF homodimer, significantly more (92 residues) of the 111 amide resonances assigned (90.2%) could be used to calculate relaxation parameters with remaining 16 resonances being significantly overlapped such that reliable estimates of signal intensity could not be determined, and two residues (53 and 54) relaxed too quickly for reliable parameters to be calculated.

The results of reduced spectral density mapping showed the N- and C- termini and the region between residues 65-70 indicate fast internal motion (τ_e) on the psec-nsec timescale. Several residues (62, 63, 74, 75, 79, 80, 92, 132 and 154) show a significant right shift in the $J(0.87\omega_H)$ *vs* J(0) plot (*i.e.,* greater than the median average deviation, see Figure S6) indicating chemical exchange in the μsec-msec timescale. These are plotted in Figure 2, main text (and see Figure S8) as a backbone representation of IL-17FF (PDB code: 3JVF).

In common with isoform IL-17AA, the N-terminal 40 residues show fast internal motions (τ_e) on the psec-nsec timescale which are moderated around the interchain disulphide bond. There are a small number of residues showing conformational exchange which are at the cystine knot, possibly due to disulphide bond isomerization, and at the bottom of the second β-hairpin that form the 'skirt' region of the dimer. However, in general terms the 'F' homodimer is a much less dynamic protein with the majority (70%) of its residue's relaxation being dominated by molecular tumbling.

Only ^{15}N labelling of the 'A' promoter of the IL-17AF hetero-dimer allowed its dynamics to be studied independently of the 'F' promoter so allowing its contribution to the function of IL-17 to be analysed (and *vice versa*). What is immediately apparent is the much more extensive relaxation data available for the 'A' protomer in the heterodimer compared to the homodimer (see Figures S3 and S8).

Nine residues (residues 66, 71, 95, 97, 120, 133, 138, 142 and 145) show a significant right shift in the $J(0.87\omega_H)$ *vs* $J(0)$ plot (Figure S6) (*i.e.,* greater than the median average deviation) indicating chemical exchange in the μsec-msec timescale. Figure 2, main text, shows a backbone representation of IL-17Af (PDB code: 5N92) colour coded using the above-described relaxation categories. Figure S8 of the Supplementary Data gives this representation of motion on the linear amino acid sequence.

The 'A' protomer has been significantly stabilized in the 'Af' hetero-dimer relative to the 'A' homodimer with more (68% for IL-17Af hetero- dimer *vs.* 26% for IL-17AA homodimer) of the backbone amides relaxation dominated by the overall correlation time of the protein. Much of the conformational exchange in the IL-17AA homodimer's N- terminal region has been stabilized, with this region now exhibiting fast internal motions (τ_e). Stabilization in this region could be due to residues 40-50 of the 'A' protomer now in close contact to residues 141-148 of the 'F' protomer. In particular, Q111 of the F protomer has polar contacts with N48 and N50 of the 'A' protomer which would help stabilize this region. The equivalent residue in the 'AA' homodimer is an arginine (R124) and therefore these stabilizing polar contacts are not possible.

However, most significant is the loss of conformational exchange in the bottom part of the second β-hairpin and the 'skirt' region. The few residues (95, 97, 120, 133, 138, 142 and 145) that are in conformational exchange are located in the loop between the two β-hairpins and in strand 4 of the second β-hairpin. Those at the top of strand 4 are in the 'collar' region of the molecular near the cysteine knot and could be a consequence of disulphide bond isomerization. The other residues are in the 'skirt' region of the molecule.

In the IL-17aF ^{15}N-TROSY spectrum, 99 resonances could be used to calculate relaxation parameters with remaining 18 resonances being significantly overlapped such that reliable estimates of signal intensity could not be determined. The dynamics of the IL-17Fa heterodimer show a very similar pattern to the IL-17FF homodimer with the N-terminal residues 49-53, 65, 66, 71 and 72 showing conformational exchange. The increased conformational exchange may be due to the loss of polar contacts these residues make with residues 143-145 with the second 'F' protomer in the homodimer. Figure 2, main text, shows a backbone representation of IL-17Fa (PDB code: 5N92) colour coded using the above described relaxation categories.

Interaction of the IL17 dimers with an inhibitory macrocycle. A series of macrocyclic ligands that inhibit the interaction of IL-17AA with IL-17RA have previously been published. In order to determine whether these ligands also interact with IL-17FF and IL-17AF we obtained NMR spectra for the IL-17 isoforms in the presence and absence of a representative macrocycle (MC). Complexing the IL-17AA homodimer and the IL-17AF heterodimer with the MC resulted in significant spectral changes consistent with high affinity binding of such a large, complex ligand. For the complex with the IL-17AA isoform many additional signals were observed in the ^{15}N-TROSY spectrum (Figure S9). These additional signals were a result of de-summarization of the dimer and, as a consequence, the spectrum could not be reliably assigned. The MC had a high enough affinity to fully saturate the IL-17AA homodimer, suggesting that the MC binds with an affinity in the order of <0.1μM. Such a tight affinity is consistent with the previously reported K_D of the MC for IL-17AA.

The MC also had high enough affinity to fully saturate the IL-17AF hetero-dimer. Interestingly, whilst there are a number of significant spectral changes in the IL-17AF TROSY spectrum, no additional signals were observed upon addition of the MC, indicating that the MC only binds in one orientation. For the IL-17FF isoform additional, but weak, signals were observed (Figure S10). This was interpreted as incomplete saturation of the binding site (estimated as about 10% based on peak height ratios) due to a combination of very low ligand affinity and the limiting solubility (c. 500uM) of the ligand. At such a low occupancy, it was not possible to obtain reliable NMR dynamics data.

To gain insight into the molecular mechanisms by which the MC inhibits the interaction of IL-17 isoforms with IL-17RA, we decided to study the effect of MC binding on both the structure and dynamics of the dimers. NMR studies focused on the interaction of IL-17AF with the MC. The large number of chemical shift changes reported upon binding MC meant that the backbone resonance assignments could not be simply transferred based on the minimal shift approach, so the NMR signals of the IL-17AF/MC complex were therefore assigned *ab initio*.

We were able to confidently assign the majority of the protein backbone of both A and F protomers in the IL-17AF isoform: 91.6% of backbone amide signals, 91.7% of Cα, 89% of Cβ and 78% of C' for the A protomer, and 95.1% of backbone amide signals, 97% of Cα, 96.8 Cβ and 88.2% of C' for the F protomer. The majority of the missing, and therefore unassigned resonances were from residues located in the N-terminal in the A chain and the loop between sheets 3 and 4 in both the A and F chains. The change in chemical shift upon macrocycle binding was mapped onto the crystal structure of IL-17AF heterodimer (PDB: 5N92, see Figure S11) so aiding the identification of the MC binding site. As can be seen, the largest chemical shift changes occur at the bottom of β-sheets 3 and 4 ('body' region) of both the 'A' and 'F' protomer. Thus, indicating the binding site is between the protomers, towards the 'skirt' of the molecule. Such a binding site is entirely constant with the crystal structure of the Il-17AA:MC complex presented here, and all published IL-17AA structures with bound ligands[14] (*e.g.,* PBDs: H5I3, H5I4, H5I5). Additionally, a double filtered NOESY spectrum was acquired on a sample of the IL-17Af:MC complex (the A protomer being labelled with ^{2}H, ^{13}C and ^{15}N) to detect NOE's between the unlabelled F protomer and the MC. Only a single set of NOEs is observed (*e.g.*, Figure S11 panel D) indicating the MC is indeed bound in a single orientation.

Effect of macrocycle (MC) binding on the backbone dynamics of IL-17AF. Addition of the MC to the IL-17AF heterodimer causes significant chemical shift changes to the spectrum however the quality of the spectrum is relatively unaffected. Of the 108 backbone amide resonances assigned in the A protomer (90.5%) 93 could be used to calculate relaxation parameters with 11 resonances being significantly overlapped such that reliable estimates of signal intensity could not be determined and 3 who's signals decayed very rapidly. Bar charts of the calculated relaxation parameters are given in Figure S3. The R_1, R_2 and hetNOE values show a similar patter to the IL-17af heterodimer in the absence of MC apart from the N- terminal region. The first 25 residues have more negative hetNOE values with residues 48-52 showing pronounced negative values. In addition, residues 53-57 could not be assigned as they were absent from the spectrum. It is assumed that these residues are broadened by significant conformational exchange.

Reduced spectral density mapping of IL-17Af:MC show the N- and C- termini have significant fast internal motion (τ_e) on the psec-nsec timescale. However, 11 residues (residues 66, 67, 72, 76, 84, 87, 93, 94, 96, 97 and 113) show a significant right shift in the $J(\omega_N)$ *vs* J(0) plot (*i.e.,* greater than the median average deviation) indicating chemical exchange in the μsec-msec timescale. Figure 2, main text, shows a backbone representation of IL-17Af:MC (PDB code: 5N92).

Binding of the MC to the heterodimer has subtle but significant effects on the dynamics of the protein. Residues L120 and I138 which in the free protein are in conformational exchange are now stabilized such their relaxation in dominated by the overall tumbling of the molecule. These two residues are in the 'skirt' region of the protein, and also map to the MC binding site with L120 forming hydrogen bonds with the MC. In addition, V142 and T145 which are in the 'collar' region of the protein by the cystine knot are also stabilized. Thus, binding of the MC would appear to have a stabilizing effect at the protomer interface. However, the base of the first β-hairpin, forming the 'sleeve' region (residues 93-94 and 96-97), is now in conformational exchange.

For the IL-17Fa:MC complex, of the 117 amide resonances assigned (95.1%) in the IL-17Fa ^{15}N-TROSY spectrum, 99 could be used to calculate relaxation parameters with remaining 17 resonances being significantly overlapped such that reliable estimates of signal intensity could not be determined and only residue 152 relaxed too quickly for reliable parameters to be calculated. Bar charts of the calculated relaxation parameters and the reduced spectral density mapping are given in Figure S3 and S5 respectively. The dynamics of the IL-17Fa:MC hetero-dimer again show a very similar pattern to both the IL-17F homo- and IL-17Fa hetero- dimer. Figure 2, main text, shows the backbone representation of IL-17Fa (PDB code: 5N92) colour coded using the above described relaxation categories. Figure S8 of the Supplementary Data gives this representation of motion on the linear amino acid sequence.

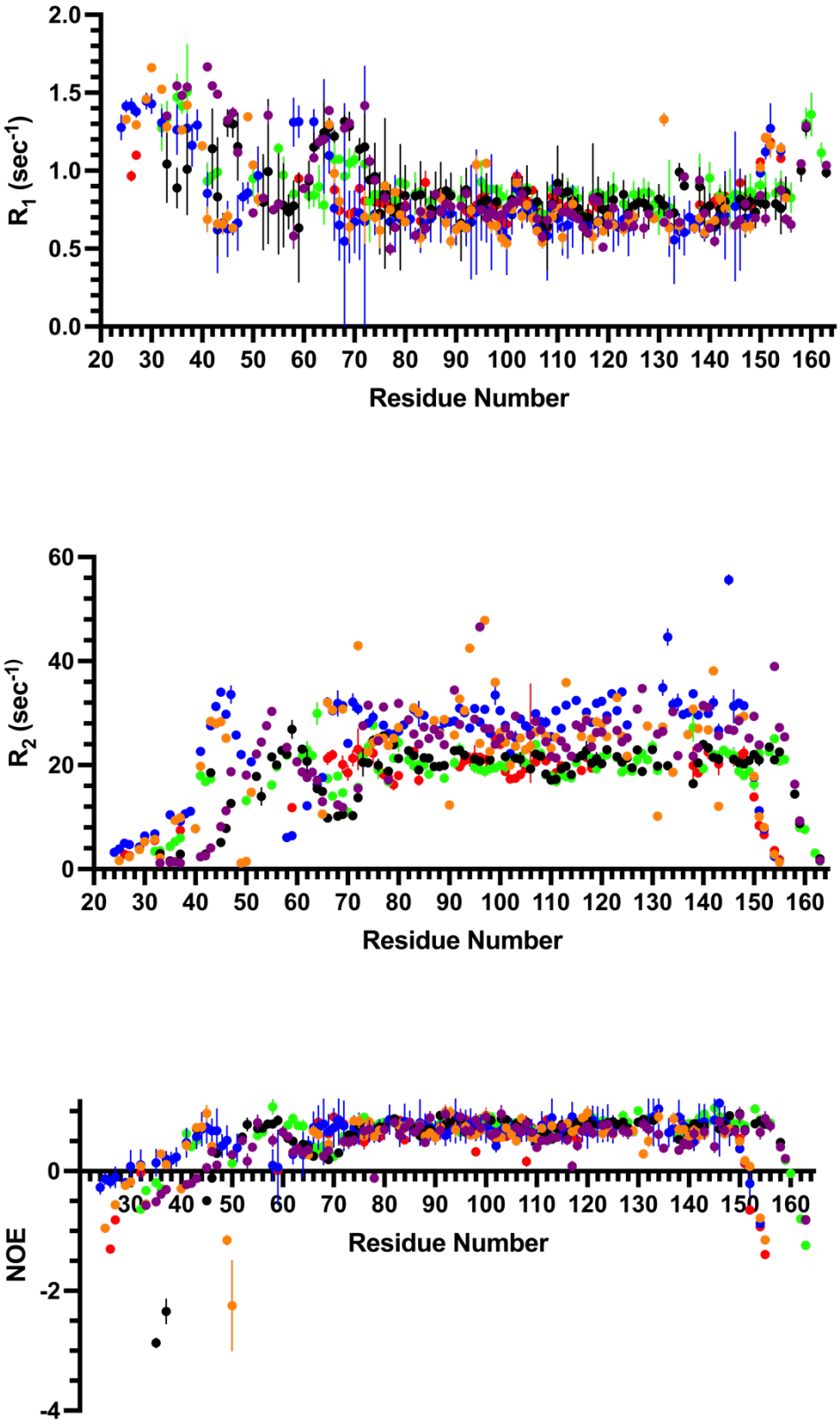

Figure S3: Plot of R_1, R_2 and 1H-15N NOE as a function of residue number. Data points are, red – IL-17AA, green – IL-17FF, blue – IL-17Af, black – IL-17Fa, orange IL-17Af:MC and purple – IL-17aF:MC

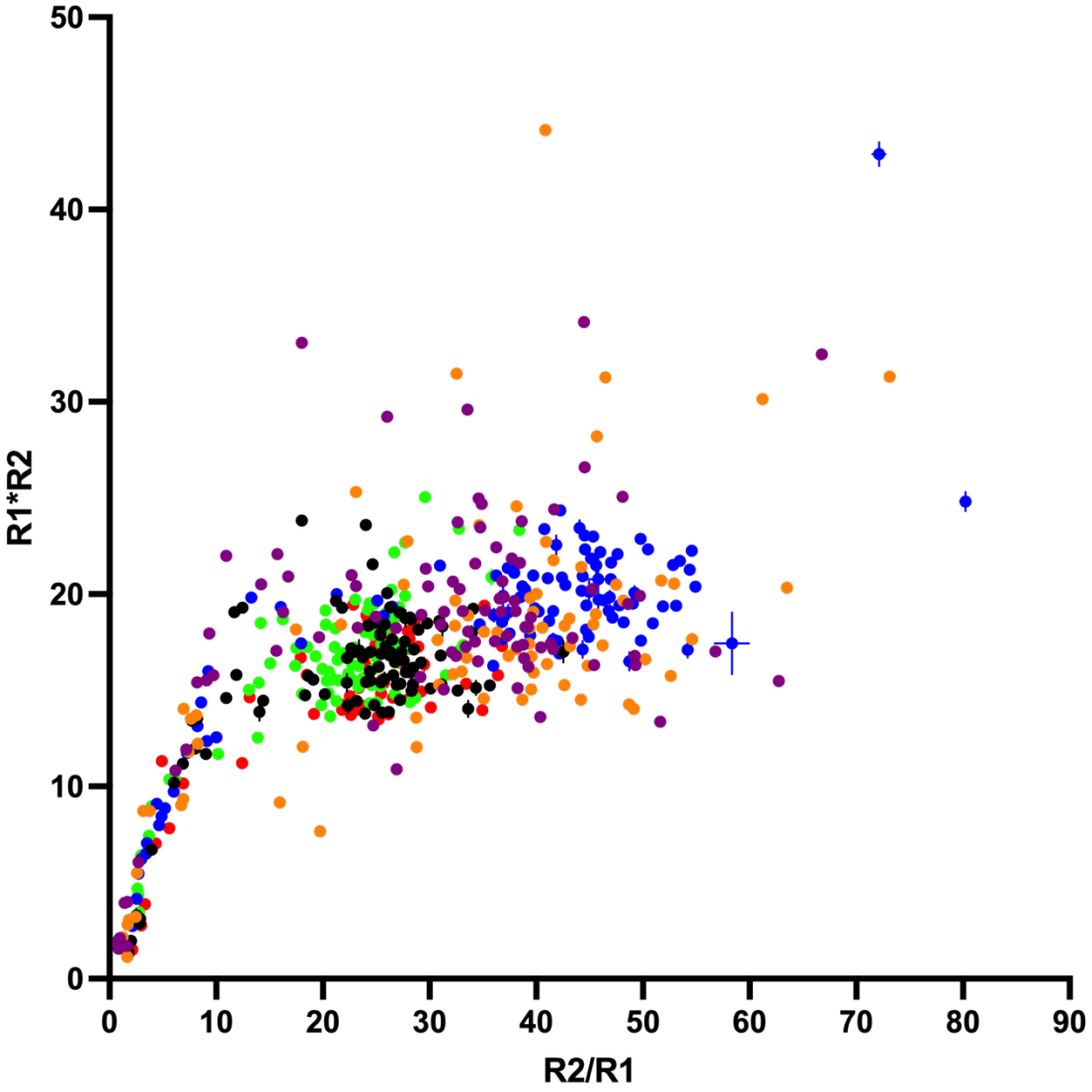

Figure S4: Plot of R_1R_2 vs R_2/R_1. Data points are, red – IL-17AA, green – IL-17FF, blue – IL-17Af, black – IL-17Fa, orange IL-17Af:MC and purple – IL-17aF:MC

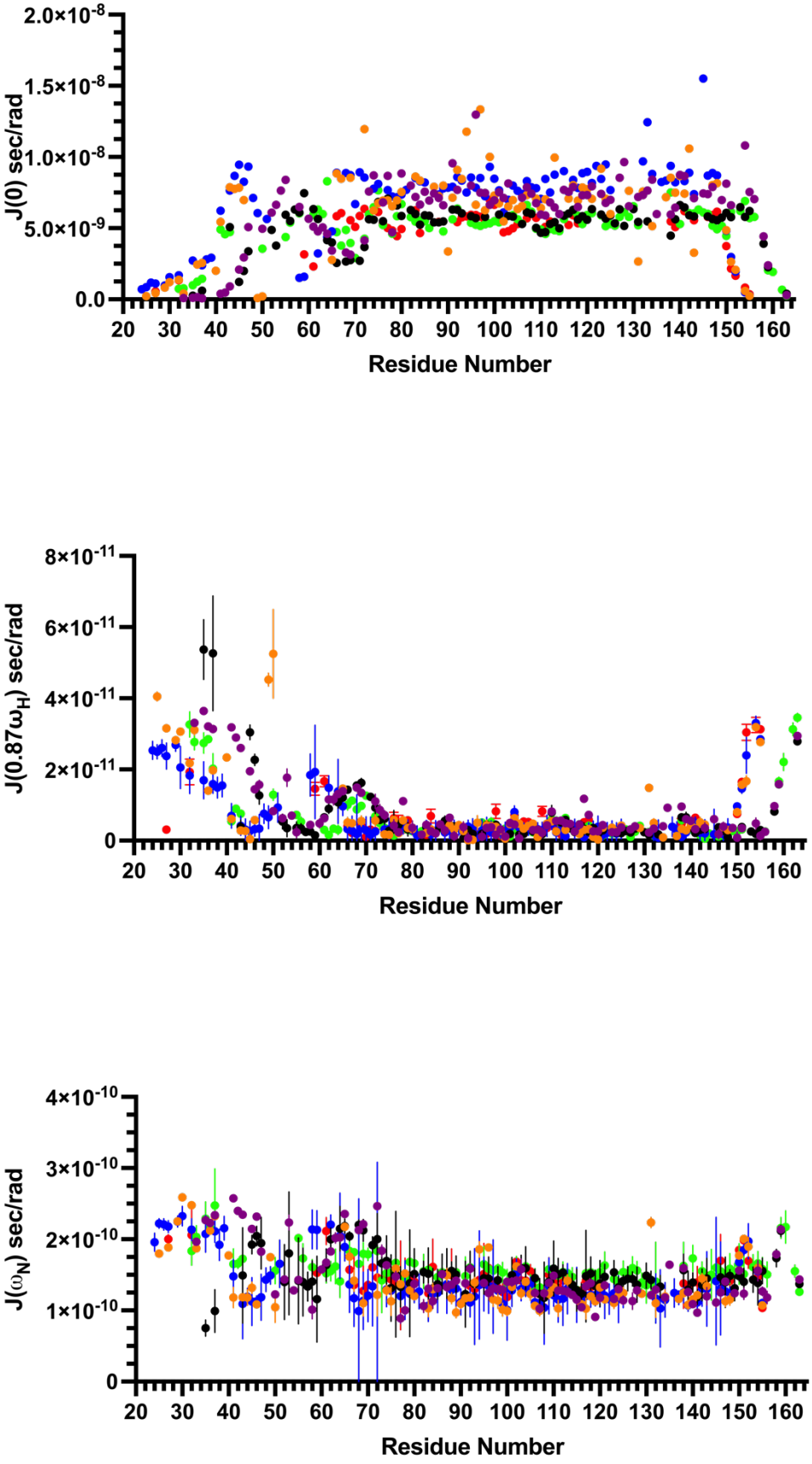

Figure S5: Plot of J(0), J(0.87ω_H) J(ω_N) and as a function of residue number. Data points are, red – IL-17AA, green – IL-17FF, blue – IL-17Af, black – IL-17Fa, orange IL-17Af:MC and purple – IL-17aF:MC

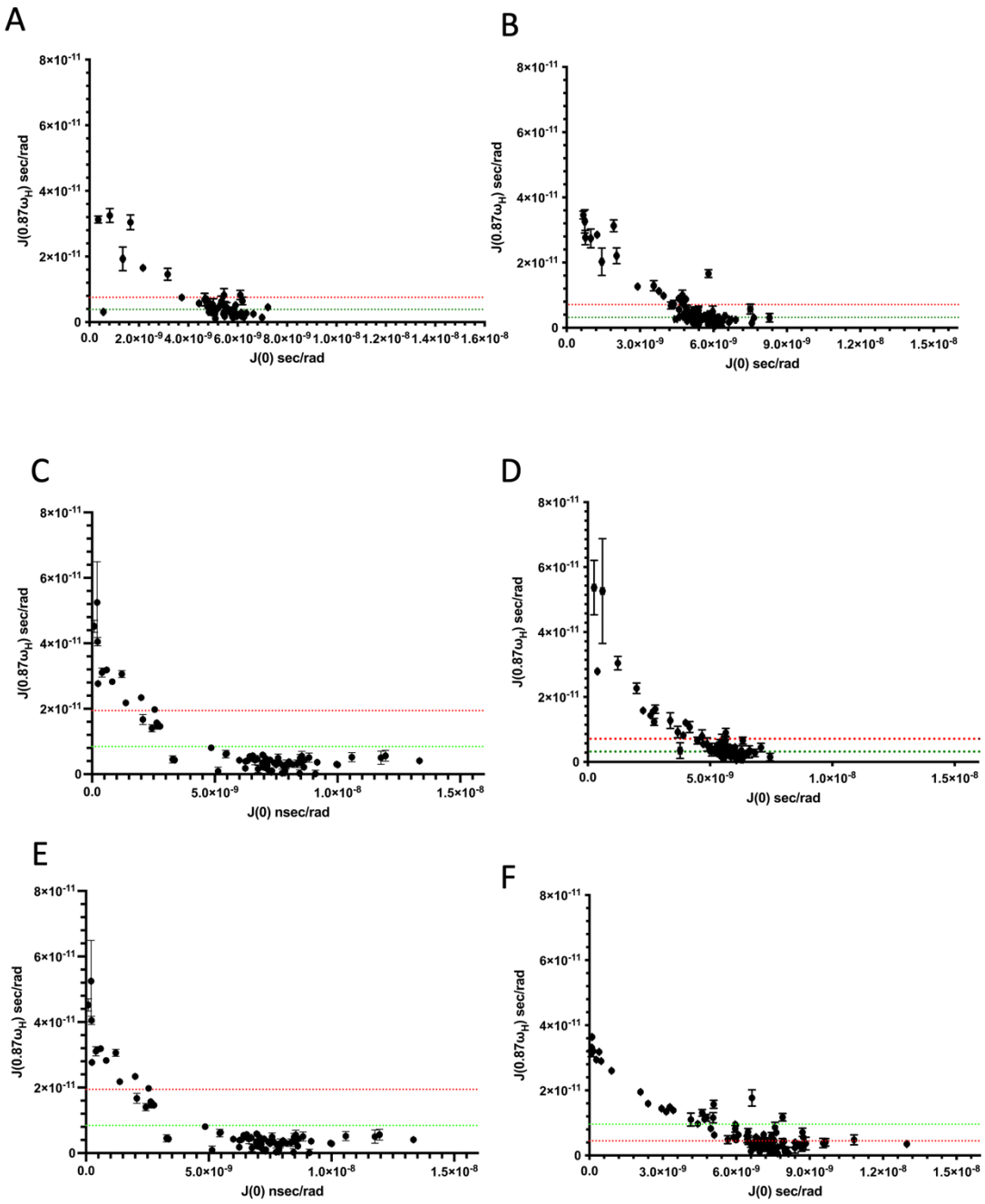

Figure S6: Plot of J(0.87ω_H) vs J(0). Panel A: IL-17AA, B: IL-17FF, C: IL-17Af, D: IL-17Fa, E: IL-17Af:MC and F: IL-17aF:MC

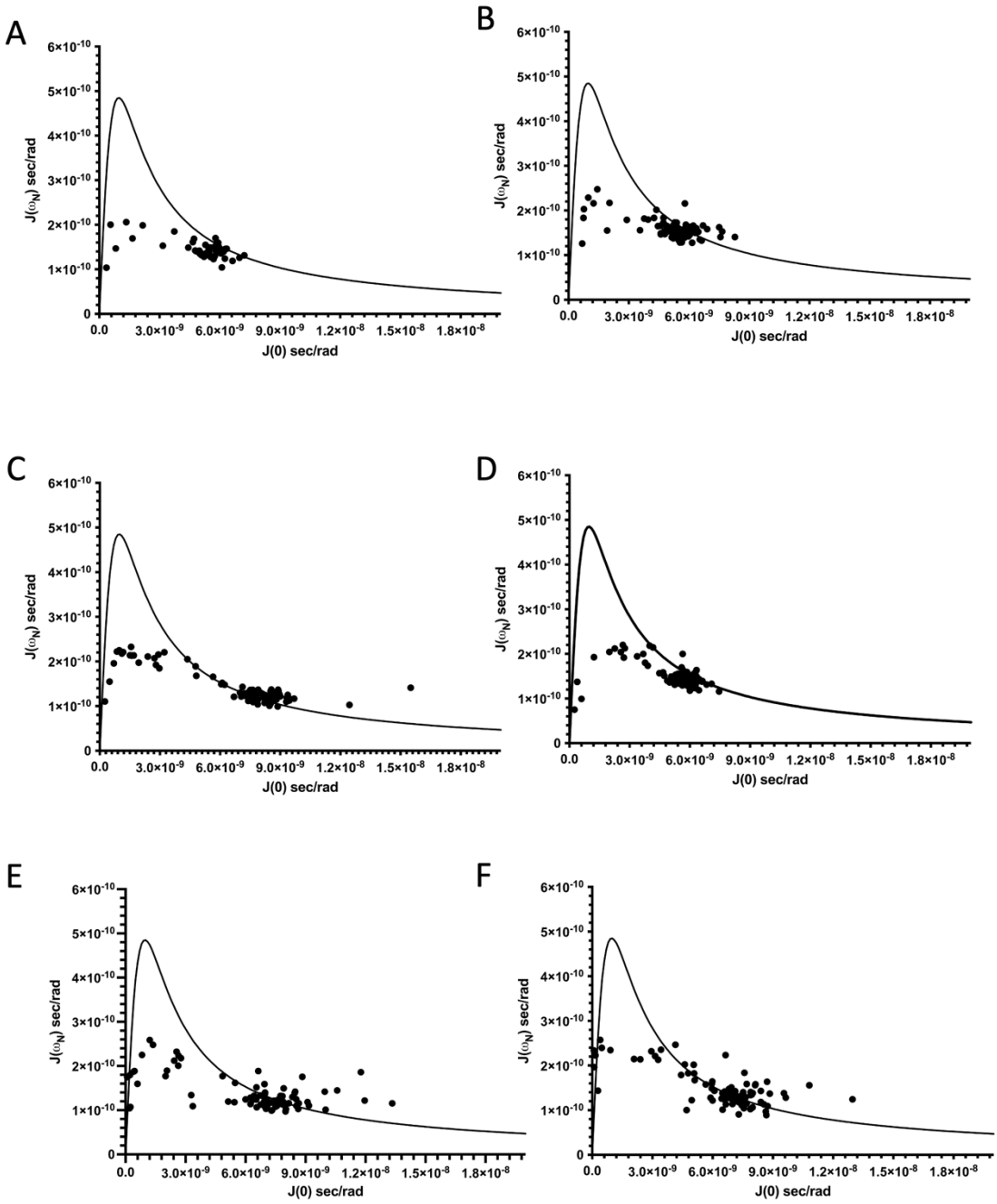

Figure S7: Plot of $J(\omega_N)$ vs $J(0)$. Panel A: IL-17AA, B: IL-17FF, C: IL-17Af, D: IL-17Fa, E: IL-17Af:MC and F: IL-17aF:MC

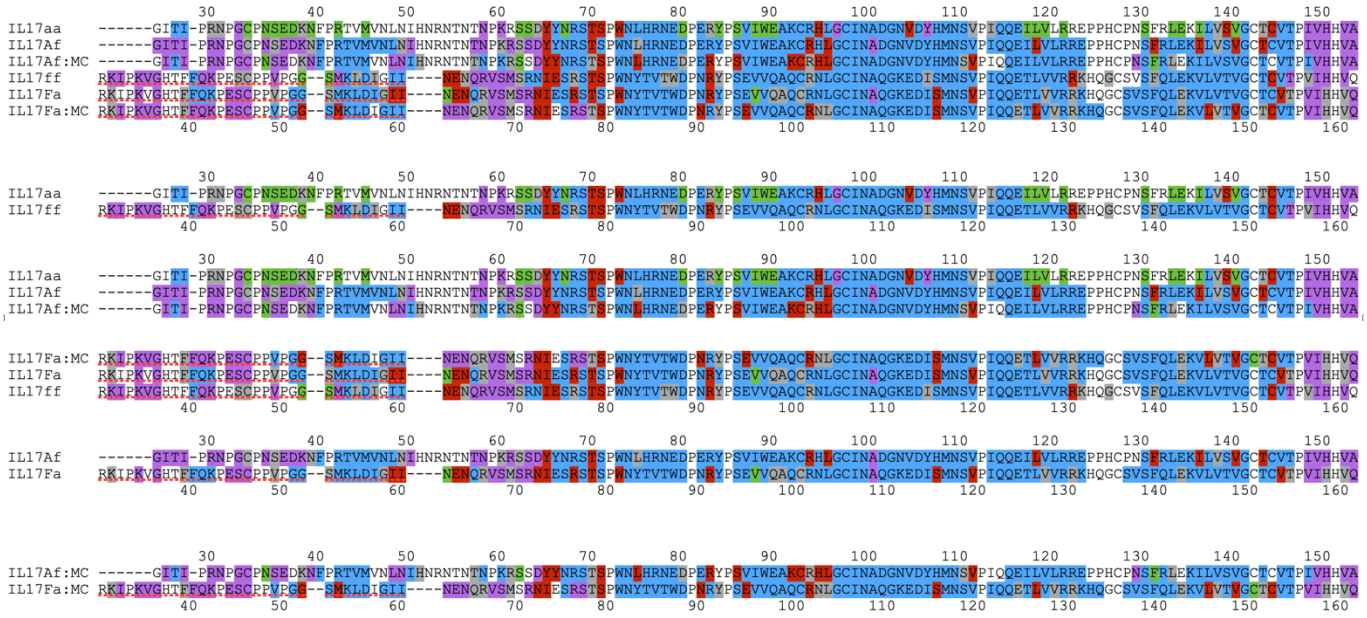

Figure S8: Primary sequence of the IL-17 protomers (aligned by secondary structure) colour coded based on relaxation being dominated by either the proteins overall correlation time (τ_c) - cyan, fast internal motions (τ_e) – purple, conformational exchange (R_{ex}) – red or assumed conformational exchange due to rapid relaxation – green. Overlapped resonances are coloured grey and no colouring are unassigned resonances.

```
PDB code 4HR9 – IL-17AA
Seq:    PRTVMVNLNI H!YYDRSTSP WNLHRNEDPE RYPSVIWEAK CRHLGCINAD      50
SS:     ccEEEEEccc ccccTTBSSc EEEEEEEcTT EESSEEEEEE EScSSEEcTT
Seq:    GNVDYHMNSV PIQQEILVLR REPPHSPNSF RLEKILVSVG CTCVTPI!PR      100
SS:     ScEETTSEEE EEEEEEEEEE ESSTTcSSEE EEEEEEEEEE EEEEcccccc
Seq:    TVMVNLNI!Y DRSTSPWNLH RNEDPERYPS VIWEAKCRHL GCINADGNVD      150
SS:     EEEEEccccc TTBSScEEEE EEEcTTEESS EEEEEEEScS SEEcTTScEE
Seq:    YHMNSVPIQQ EILVLRREPP HSPNSFRLEK ILVSVGCTCV TP              192
SS:     TTSEEEEEEE EEEEEEESST TcSSEEEEEE EEEEEEEEEE cc

Percentage of amino acids in the different secondary structures in:
H       G       I       E       B       T       S       coil
0.0%    0.0%    0.0%    57.3%   1.0%    10.4%   13.5%   17.7%


PDB code 1JPY – IL-17FF
Seq:    HTFFQKPESC PPVPGGSMKL DIGIINENQR VSMSRNIESR STSPWNYTVT      50
SS:     cGGGcccTTS cccSSSEEEE EEEEETTTcc ccccTTHHHH BSScEEEEEE
Seq:    WDPNRYPSEV VQAQCRNLGC INAQGKEDIS MNSVPIQQET LVVRRKHQGC      100
SS:     EcTTEESSEE EEEEEScSSE EcSSScEETT SEEEEEEEEE EEEEEESSGG
Seq:    SVSFQLEKVL VTVGCTCVTP V!HTFFQKPE SCPPVPGGSM KLDIGIINEN      150
SS:     GcEEEEEEEE EEEEEEEcc cccTTScccS SScccGGGcE EEEEEEETTT
Seq:    QRVSMSRNIE SRSTSPWNYT VTWDPNRYPS EVVQAQCRNL GCINAQGKED      200
SS:     ccccccTTHH HHBSScEEEE EEEcTTEESS EEEEEEEScS EEEcTTScEE

Percentage of amino acids in the different secondary structures in:
H       G       I       E       B       T       S       coil
2.5%    2.5%    0.0%    47.7%   1.4%    11.0%   12.6%   22.3%


PDB code 5N92 – IL-17AF
Seq:    KNFPRTVMVN LNIHNRNTN! SDYYNRSTSP WNLHRNEDPE RYPSVIWEAK      50
SS:     ccccSEEEEE SccEEcSccc ccHHHHBSSc EEEEEEEcTT EESSEEEEEE
Seq:    CRHLGCINAD GNVDYHMNSV PIQQEILVLR REPPHCPNSF RLEKILVSVG      100
SS:     EScSSEEcTT SSEETTSEEE EEEEEEEEEE ESSTTcSSEE EEEEEEEEEE
Seq:    CTCVTPIVHH !PESCPPVPG GSMKLDIGII NENQRVSMSR NIESRSTSPW      150
SS:     EEEEcSScccc ccccccccccT TEEEEEEccS STTccTTTTc cHHHHBSScE
Seq:    NYTVTWDPNR YPSEVVQAQC RNLGCINAQG KEDISMNSVP IQQETLVVRR      200
SS:     EEEEEEcTTE EScEEEEEEE ScSSEEcSSS cEETTSEEEE EEEEEEEEEE
Seq:    KHQGCSVSFQ LEKVLVTVGC TCVTPVIHHV Q                          231
SS:     EESSScEEEE EEEEEEEEEE EEEccccccc c

Percentage of amino acids in the different secondary structures in:
H       G       I       E       B       T       S       coil
3.5%    0.0%    0.0%    50.2%   0.9%    8.7%    14.7%   22.1%

PDB code 8CDG – IL-17AA plus MC
Seq:    PRTVMVNLNI H!YYDRSTSP WNLHRNEDPE RYPSVIWEAK CRHLGCINAD      50
SS:     ccEEEEEcSc cccccSBSSc EEEEEEEcTT EESSEEEEEE EScSSEEcTT
Seq:    GNVDYHMNSV PIQQEILVLR REPPHSPNSF RLEKILVSVG CTCVTPI!PR      100
SS:     ScEETTSEEE EEEEEEEEEE ESSTTcSSEE EEEEEEEEEE EEEEcccccc
Seq:    TVMVNLNI!Y DRSTSPWNLH RNEDPERYPS VIWEAKCRHL GCINADGNVD      150
SS:     EEEEEccccc TTBSScEEEE EEEcTTEESS EEEEEEEScS SEEcTTScEE
Seq:    YHMNSVPIQQ EILVLRREPP HSPNSFRLEK ILVSVGCTCV TP!X            194
SS:     TTSEEEEEEE EEEEEEESST TcSSEEEEEE EEEEEEEEEE cccc

Percentage of amino acids in the different secondary structures in:
H       G       I       E       B       T       S       coil
0.0%    0.0%    0.0%    56.7%   1.0%    9.3%    14.4%   18.6%
```

Figure S9: Summarised DSSP output for the four crystal structures used during this study. There are no obvious differences in the secondary structural elements of the structures used during this study, particularly when the difference in construct length and the data completeness are considered (*i.e.*, different crystal structures were able to resolve different lengths and sections of the peptide backbone and contained different binding partners such as peptides or antibodies).

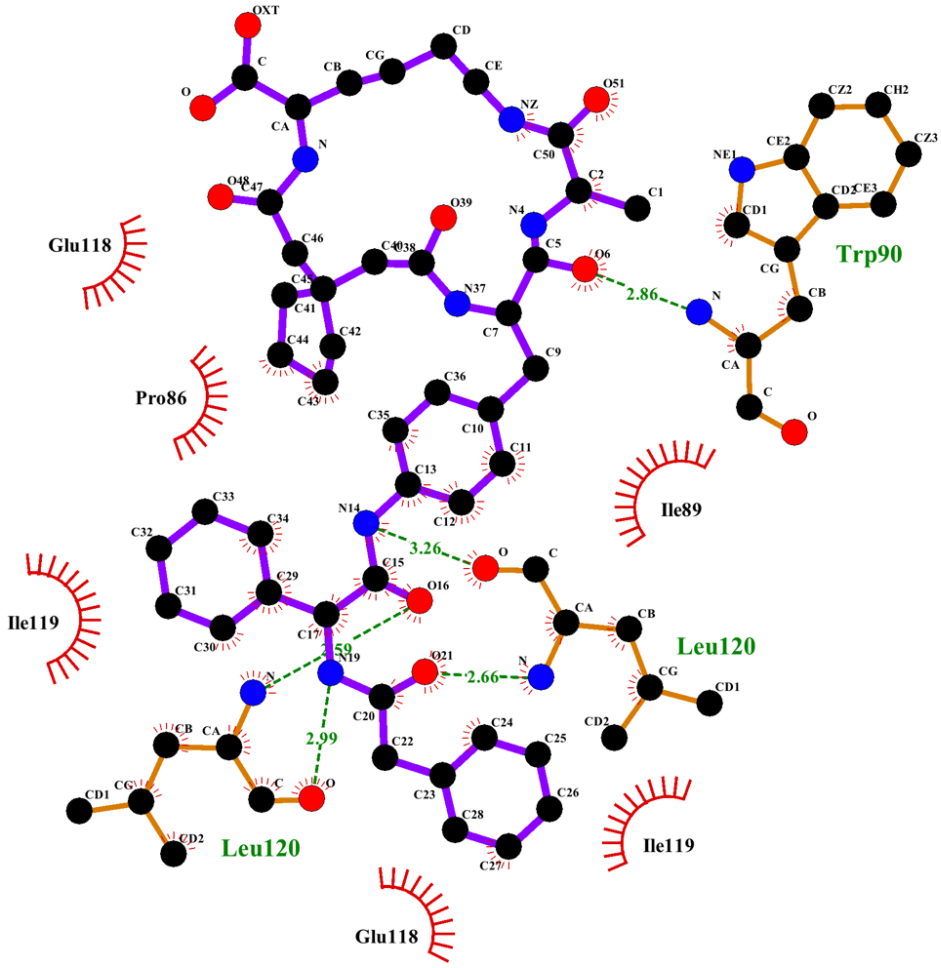

Figure S10: LigPlot+[2] representation of the Macrocycle interactions with IL-17AA showing the hydrogen bonding network (green dotted line) and hydrophobic interactions (red).

Data collection	
Space group	$C222_1$
Resolution range (Å)	29.39-2.90 (2.98-2.90)[a]
Unit cell dimensions	
a,b,c (Å)	67.36, 89.77, 116.67
α,β,γ (°)	90, 90, 90
Wavelength (Å)	0.9282
No. molecules in asymmetric unit	1
Completeness (%)	99.5 (98.9)
Multiplicity	6.5 (6.7)
R_{merge}	0.068 (0.930)
Mean I/σI	22.5 (1.9)
Refinement	
Resolution range (Å)	29.39-2.90 (3.32-2.90)
No. reflections	8060 (2477)
R_{work}/R_{free}	0.2482/0.2851
No. non-H atoms overall	1589
protein	1532
ligands	57
Average B-factor (Å^2) overall	86.75
protein	87.19
ligands	74.83
Geometry	
R.m.s. deviation bond lengths (Å)	0.011
R.m.s. deviation bond angles (°)	1.556

[a]Statistics in the highest resolution bin are shown in parenthesis.

Table S1. Data collection and refinement statistics.

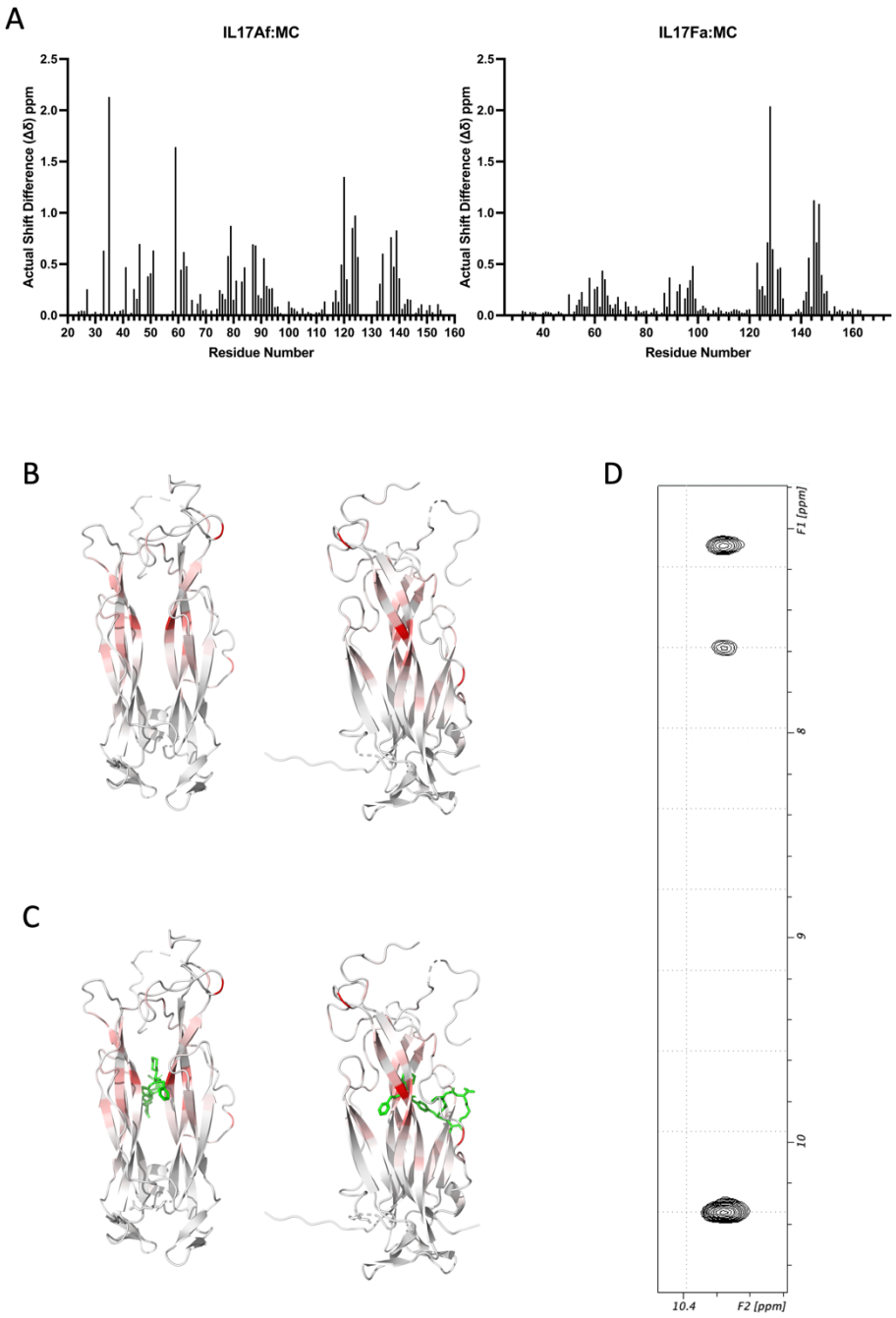

Figure S11: Chemical shift changes to IL-17AF upon MC binding. Panel A, bar chart of the actual chemical shift difference (Δδ) of the A and F protomer between apo and when bound to the MC. Panel B, ribbon representation of the boackbone of the IL-17AF isoform (PDB code: 5N92) colour coded with a white to red gradient of actual shift, with no shift being white and the largest shift being red. Panel C, as panel B but rotated 90° left to right and overlayed with the crystal structure of the IL-17AA isoform bound to MC solved in this study. Panel D, $^{15}N/^{13}C$ double filtered NOESY spectrum of IL-17Af:MC, strip shows NOEs from the indole of W81 of the F protomer to the amides of the MC. The single set of NOEs indicates the MC is present in a single orientation.

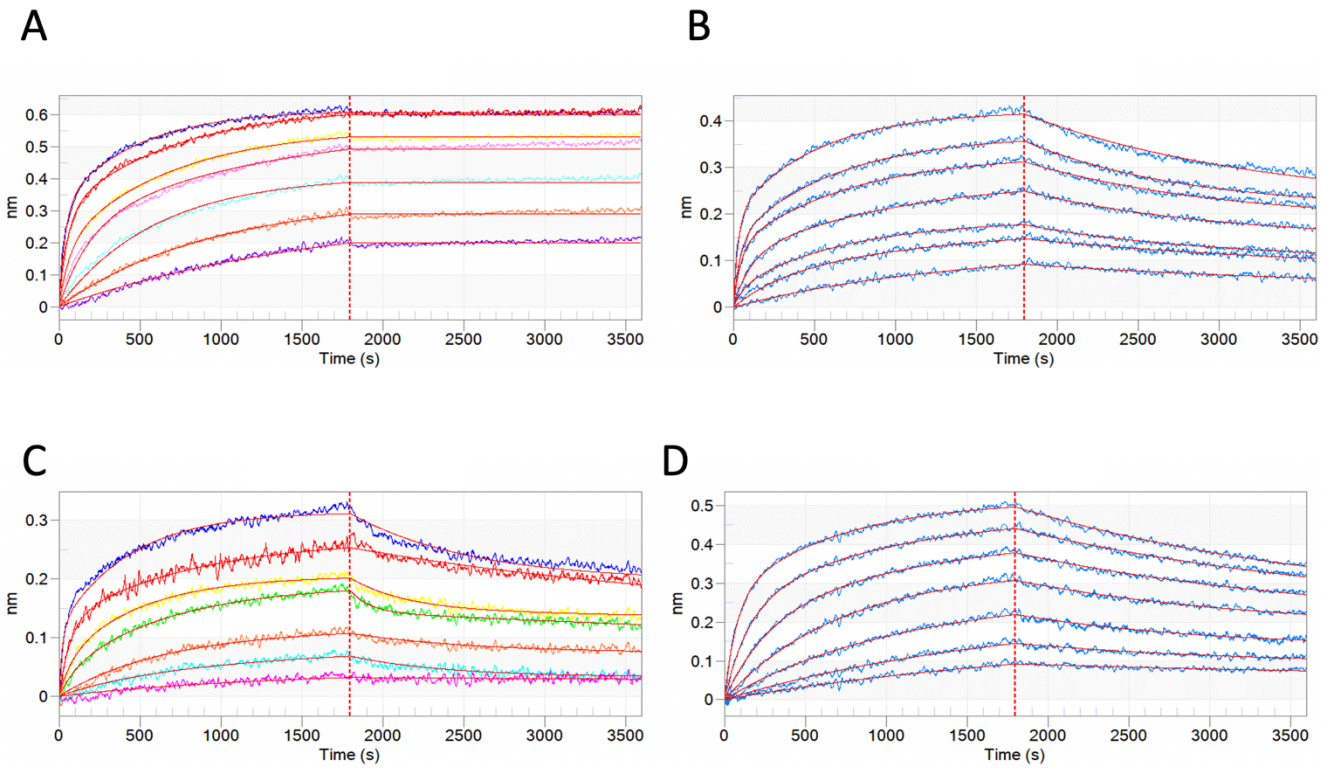

Figure S12 Representative binding isotherms from Biolayer Interferometry Binding Assays. A) IL-17AA alone with IL-17RA B) IL-17AF alone with IL-17RA C) IL-17AA:MC complex with IL-17RA D) IL-17AF:MC complex with IL-17RA.

1. Minnes, L.; Shaw, D. J.; Cossins, B. P.; Donaldson, P. M.; Greetham, G. M.; Towrie, M.; Parker, A. W.; Baker, M. J.; Henry, A. J.; Taylor, R. J.; Hunt, N. T., Quantifying Secondary Structure Changes in Calmodulin Using 2D-IR Spectroscopy. *Anal Chem* **2017,** *89* (20), 10898-10906.
2. Laskowski, R. A.; Swindells, M. B., LigPlot+: multiple ligand-protein interaction diagrams for drug discovery. *J Chem Inf Model* **2011,** *51* (10), 2778-86.
3. Waters, L. C.; Veverka, V.; Strong, S. L.; Muskett, F. W.; Dedi, N.; Lawson, A. D. G.; Prosser, C. E.; Taylor, R. J.; Henry, A. J.; Carr, M. D., Conformational dynamics in interleukin 17A and 17F functional complexes is a key determinant of receptor A affinity and specificity. *Cytokine* **2021,** *142*, 155476.
4. Cavanagh, J., Fairbrother, W.J., Palmer III, A.G., Rance, M. and Skleton, N.J., *Protein NMR Spectroscopy: Principles and Practice* 2nd ed.; Academic Press: 2007; p 587.
5. Piotto, M.; Saudek, V.; Sklenar, V., Gradient-Tailored Excitation for Single-Quantum Nmr-Spectroscopy of Aqueous-Solutions. *Journal of biomolecular NMR* **1992,** *2* (6), 661-665.
6. Zwahlen, C.; Legault, P.; Vincent, S. J. F.; Greenblatt, J.; Konrat, R.; Kay, L. E., Methods for measurement of intermolecular NOEs by multinuclear NMR spectroscopy: Application to a bacteriophage lambda N-peptide/boxB RNA complex. *Journal of the American Chemical Society* **1997,** *119* (29), 6711-6721.
7. Zhu, G.; Xia, Y.; Nicholson, L. K.; Sze, K. H., Protein dynamics measurements by TROSY-based NMR experiments. *J Magn Reson* **2000,** *143* (2), 423-6.
8. Lakomek, N. A.; Ying, J. F.; Bax, A., Measurement of N-15 relaxation rates in perdeuterated proteins by TROSY-based methods. *Journal of biomolecular NMR* **2012,** *53* (3), 209-221.
9. Delaglio, F.; Grzesiek, S.; Vuister, G. W.; Zhu, G.; Pfeifer, J.; Bax, A., NMRPipe: a multidimensional spectral processing system based on UNIX pipes. *Journal of biomolecular NMR* **1995,** *6* (3), 277-93.
10. Lee, W.; Tonelli, M.; Markley, J. L., NMRFAM-SPARKY: enhanced software for biomolecular NMR spectroscopy. *Bioinformatics* **2015,** *31* (8), 1325-7.
11. Farrow, N. A.; Muhandiram, R.; Singer, A. U.; Pascal, S. M.; Kay, C. M.; Gish, G.; Shoelson, S. E.; Pawson, T.; Formankay, J. D.; Kay, L. E., Backbone Dynamics of a Free and a Phosphopeptide-Complexed Src Homology-2 Domain Studied by N-15 Nmr Relaxation. *Biochemistry* **1994,** *33* (19), 5984-6003.
12. d'Auvergne, E. J.; Gooley, P. R., Optimisation of NMR dynamic models II. A new methodology for the dual optimisation of the model-free parameters and the Brownian rotational diffusion tensor. *Journal of biomolecular NMR* **2008,** *40* (2), 121-33.
13. d'Auvergne, E. J.; Gooley, P. R., Optimisation of NMR dynamic models I. Minimisation algorithms and their performance within the model-free and Brownian rotational diffusion spaces. *Journal of biomolecular NMR* **2008,** *40* (2), 107-19.
14. Liu, S.; Dakin, L. A.; Xing, L.; Withka, J. M.; Sahasrabudhe, P. V.; Li, W.; Banker, M. E.; Balbo, P.; Shanker, S.; Chrunyk, B. A.; Guo, Z.; Chen, J. M.; Young, J. A.; Bai, G.; Starr, J. T.; Wright, S. W.; Bussenius, J.; Tan, S.; Gopalsamy, A.; Lefker, B. A.; Vincent, F.; Jones, L. H.; Xu, H.; Hoth, L. R.; Geoghegan, K. F.; Qiu, X.; Bunnage, M. E.; Thorarensen, A., Binding site elucidation and structure guided design of macrocyclic IL-17A antagonists. *Sci Rep* **2016,** *6*, 30859.